Noncontact Dipole Effects on Channel Permeation. V. Computed Potentials for Fluorinated Gramicidin

Dean G. Anderson,* Randall B. Shirts,† Timothy A. Cross,‡ and David D. Busath*
*Zoology Department and Center for Neuroscience and †Department of Chemistry and Biochemistry, Brigham Young University, Provo, Utah 84602, and ‡Center for Interdisciplinary Magnetic Resonance at the National High Magnetic Field Laboratory, Institute of Molecular Biophysics and Department of Chemistry, Florida State University, Tallahassee, Florida 32306 USA

ABSTRACT Experimental and theoretical calculations indicate that the dipole moment of the four Trp side chains in gramicidin A (gA) channels modify channel conductance through long-range electrostatic interactions. Electrostatic ion/side-chain interaction energies along the channel were computed with CHARMM using ab initio atom charges for native and 4-, 5-, or 6-fluorinated Trp side chains. The bulk water reaction to the polar side chains was included using the method of images as implemented by Dorigo et al. (1999), and channel waters in idealized structures were included. Ion/Trp interaction energies were ~ -0.6 kcal/mol throughout the channel for all four of the native Trp pairs. Channel waters produced a modest reduction in the magnitude of interactions, essentially offsetting images representing the bulk water outside the channel. The effects of side-chain fluorination depended on ring position and, to a lesser extent, residue number. Compared with native Trp, 5-fluorination reduces the translocation barrier with minor effects on the exit barrier. In contrast, 6-fluorination primarily reduces exit barrier. 4-Fluorination produces a more complex double-well energy profile. Effects of measured side-chain movements resulting from fluorination or change in lipid bilayer were negligible whereas thermal side chain librations cause large effects, especially in the region of the ion-binding sites.

INTRODUCTION

Fluorinated amino acids have been introduced into proteins as a small, useful perturbation to help analyze structure and dynamics. Nearly isosteric with hydrogen but heavier and more electronegative, fluorine often modifies dipole potentials with only modest effects on structure or dynamics (e.g., De Wall et al., 2000). Gramicidin channels (Busath, 1993; Killian, 1992; Woolley and Wallace, 1992) are a useful model of narrow cation-selective membrane channels for analyzing the effects of structural and/or electrostatic changes near the current pathway. Fluorination effects have been explored in gramicidin channels. For instance, fluorination of Val-1 near the center of the channel (Russell et al., 1986) introduces novel gating and modulates permeation by way of through-space dipole potentials (Koeppe et al., 1990).

The gramicidin channel consists of a head-to-head dimer of $\beta^{6.5}$ helices in which the 4-Å pore is lined by the neutrally terminated peptide backbone. There are ion-binding sites just inside the channel at each end according to NMR of micelles (Urry et al., 1982), x-ray diffraction (Olah et al., 1991), solid-state NMR (Tian and Cross, 1999), and molecular dynamics computations (Roux et al., 1995). These sites appear to be diffuse loci where there is a balance between hydration and peptide coordination forces on the ions. The pore provides a polar, aqueous pathway for ion translocation across the hydrophobic bilayer. Passage of cations from one binding site through the channel to the other (translocation) is limited by the mobility of the waters in the channel, the electrostatic pull of the ion-oriented waters from the bath, and the electrostatic potential from the lipid-water interface (e.g., see Cifu et al., 1992). Translocation is rate limiting at high ion concentrations as evidenced by a shift to superlinear current-voltage relations (Hladky and Haydon, 1984). Cation exit, which is slowed by strong coordination forces from peptide carbonyls, appears to be limiting at intermediate concentrations (i.e., above the first-ion dissociation constants, 0.04–0.08 M). Electrodiffusive collision with the entry limits the current through the channel at low bath concentrations, <0.1 M (Andersen, 1983). These three limitations can be conceptualized as energy barriers in the Eyring rate theory tradition, although in some cases they clearly derive from a different mechanism, such as diffusion-limited association (Hladky, 1999). Nevertheless, perturbations in the free energy at key points in the permeation process (the entry, the binding site, and the center of the channel where the translocation barrier is assumed to peak) should affect the rates of ion movement into, between, and out of the two binding sites according to the Boltzmann theorem as utilized in rate theory. The purpose of this paper is to report electrostatic computations of the ion side-chain interaction energies expected to modulate these rates for use in either kinetic or electrodiffusion analyses.

The side chains, which project radially from the backbone, are all hydrophobic. Four Trp side chains (residues 9, 11, 13, and 15) are known to enhance channel conductance relative to Phe analogs (Heitz et al., 1986, 1988; Becker et

Received for publication 3 January 2000 and in final form 19 September 2000.

Address reprint requests to Dr. David Busath, Zoology Department and Center for Neuroscience, Brigham Young University, Provo, UT 84602. Tel.: 801-378-8753; Fax: 801-378-7423; E-mail: David_Busath@BYU.edu.

0006-3495/01/09/1255/10 $2.00

al., 1991; Fonseca et al., 1992), presumably via through-space dipole potentials (Becker et al., 1991; Hu and Cross, 1995). Recent work has focused on the effect of fluorination of Trp side chains near the channel entry and exit on channel conductance (Andersen et al., 1998; Busath et al., 1998; Cotten et al., 1999; Fairbanks et al., 1999; Phillips et al., 1999; Thompson et al., 2001).

In dimyristoylphosphatidylcholine (DMPC) multilayers, solid-state nuclear magnetic resonance shows that fluorination of the Trp side chains (Cotten et al., 1999) has little effect on side-chain position. For 5- and 6-fluorination of the Trp 11, 13, and 15 indoles, for which splitting of the deuterium resonances were sharp enough that assignments were possible, the splitting magnitudes could be used to determine the changes in side-chain dihedrals. In these three cases, 5- or 6-fluorination caused changes in χ_1 of 1–5° and changes in χ_2 of 1–12°.

In channel conductance experiments, 5-fluorination of the Trp_{13} indole enhances alkali metal cation conductance in painted diphytanoylphosphatidylcholine (DPhPC) bilayers (Andersen et al., 1998; Busath et al., 1998) but reduces it in painted glyceryl monoolein (GMO) bilayers (Busath et al., 1998) (and reduces proton conductance in both types of bilayer (Phillips et al., 1999)). Preliminary rate theory analysis indicates that these contradictory effects on alkali metal cation conductances in the two types of bilayers may be explained by differences in the underlying potential energy profile deriving from the interfacial dipole potentials (Thompson et al., 2001). Furthermore, this rate theory analysis is consistent with the interpretation of Hu and Cross (1995) that Trp dipole potentials primarily affect the height of the translocation barrier peak located in the center of the channel.

The shape and magnitude of the Trp dipole potentials along the channel axis are expected, based on simplified models and atomic simulations, to depend on side-chain conformation as recently reviewed in Dorigo et al. (1999). The NMR-derived conformations (Arsenyev et al., 1990; Hu et al., 1993, 1995; Koeppe et al., 1994, 1995, 1996) are well defined for three of the four Trps and narrowed to two discrete possibilities for Trp_9. In all cases, the side-chain dipole moment is roughly parallel to the channel axis and is expected to contribute a broad well to the transport free energy profile (Sancho and Martínez, 1991), although there is controversy from atomistic modeling over whether the Trp contribution is a single well spanning the entire channel (Dorigo et al., 1999) or a pair of wells localized near the two ion-binding sites (Woolf and Roux, 1997).

Fluorination of the Trp side chain is expected from ab initio calculations to modify the indole dipole magnitude and orientation, as discussed recently in Cotten et al. (1999). Fluorination at the indole C5 position increases the dipole moment by 90%, with little effect on dipole orientation relative to the common heterocycle bond (an 8° rotation in the plane of the indole (Cotten et al., 1999)). In contrast, fluorination at position C6 rotates the dipole 35° toward the long axis of the indole, with less effect (45% increase) on the dipole magnitude. Substitution at C4 rotates the dipole in the opposite direction (i.e., by −16°) and increases the magnitude by 70%. Here we report the side-chain electrostatic contributions to the gA axial potential energy profile for fluorinated and non-fluorinated Trp side chains computed using ab initio partial charges on the side chains (Cotten et al., 1999) with a static gramicidin structure obtained by refinement from solid-state NMR (Ketchem et al., 1997). This will be useful for interpretation of currents mediated by K^+, which is predicted by theory to remain on axis (Kim et al., 1985). We first utilized the refined solid-state NMR positions for the Trp side chains (Ketchem et al., 1997) and then examined the effects of slight modifications of position subsequently measured for the fluorinated compounds (Cotten et al., 1999).

The effect of ion position on side-chain structure was not explored. Because the side-chain position measured by solid-state NMR varies negligibly upon occupancy of the ion-binding site by Na^+ (Tian et al., 1996; Tian and Cross, 1999), it seems likely that effects of the ion on side-chain structure are minimal throughout the reaction coordinate. As in the related paper in this series (Dorigo et al., 1999), our calculation included image charges in the bulk aqueous baths to represent the polarization of the bath dipoles by the side chains. This approach does not include ionic strength effects, which are expected to be small.

In addition, we have added ordered channel waters on either side of the probe ion to allow an estimate of the upper limit of the effect of interactions between polar side chains and waters ordered by the ion in the channel on the permeation free energy profile. The waters were ordered in two extreme patterns. The first is a herringbone pattern in which each water dipole points directly away from the ion, the dipole forming an angle of 0° or 180° with the channel axis. The second is a channel hydrogen-bonded pattern in which each water forms hydrogen bonds with the water behind it and the channel wall, the dipole forming an angle of 52.25° with the channel axis. According to recent molecular dynamics computations, water in the channel with one ion present is ordered between these two extremes, approaching the herringbone pattern nearest the ion and the channel hydrogen-bonded pattern four to five waters from the ion (Duca and Jordan, 1998). To take any axial anisotropy (due to the backbone and side chains) into account, we computed average interaction energies for a group of 30° axial rotations of the water columns and represent the anisotropy by showing the group standard deviation as variation bars in the computed profiles. Finally, to explore how much plasticity there might be in these potentials inherent in the side-chain flexibility, we ask whether side-chain librations of the magnitude estimated from solid-state NMR (Hu et al., 1995) would cause a qualitative change in the free energy profile contribution.

TABLE 1 Partial charges on Trp side chains

Indole names	Trp names	Trp	4F-Trp	5F-Trp	6F-Trp
(H3)	Cβ	0.218*	0.205	0.201	0.202
C3	Cγ	−0.468	−0.341	−0.379	−0.386
C2	Cδ1	−0.070	−0.149	−0.209	−0.160
C8	Cδ2	0.255	0.024	0.347	0.161
N1	Nε1	−0.380	−0.285	−0.200	−0.275
C9	Cε2	0.237	0.223	0.002	0.217
C4	Cε3	−0.288	0.367	−0.586	−0.189
C7	Cξ2	−0.370	−0.419	−0.170	−0.579
C5	Cξ3	−0.211	−0.426	0.566	−0.470
C6	Cη2	−0.086	−0.033	−0.447	0.587
–	Hβ1	0	0	0	0
–	Hβ2	0	0	0	0
H2	Hδ1	0.175	0.191	0.213	0.195
H	Hε1	0.338	0.320	0.296	0.320
H(F)4	H(F)ε3	0.179	−0.230	0.251	0.186
H7	Hζ2	0.186	0.198	0.176	0.248
H(F)5	H(F)ζ3	0.152	0.210	−0.284	0.223
H(F)6	H(F)η2	0.133	0.144	0.224	−0.279
μ_{QM}(D)[†]		2.097	3.571	3.984	3.048
μ_{PC} (D)[‡]		2.070	3.565	3.978	3.052
$\mu_{1mag'}$ (D)[§]		2.0	3.2	3.6	2.8

*Although six decimal places were computed and used for the partial charges in the calculations to assure a neutral side chain, only the first three are reliable for the grid used in the electrostatic fitting.

[†]The net dipole moment of the indolic compounds computed directly from the 6-311G* computation.

[‡]The net dipole computed from the partial charges obtained by fitting the electrostatic potential, atoms positioned at the *ab initio* locations.

[§]The average dipole moment of the four indolic side chains as implemented for the potential energy calculations: atoms at the 1mag positions except for fluorine and Cβ as described in Methods.

METHODS

Charges and parameters

Partial charges for the Trp and fluorinated Trp side chains were derived from ab initio calculations done at the 6–311G** HF level for indole and fluorinated indole derivatives. The computations were performed with SPARTAN (Release 4.1.2, Wavefunction, Irvine, CA) and included gas-phase geometry optimization and fitting of atomic partial charges to best match the electrostatic potential on a fine (>5000-point) grid. Details of the method used and comparison of partial charges and geometries with those done by others were reported previously for indole, 5F-indole, and 6F-indole (Cotten et al., 1999). In Table 1 we report the partial charges for these compounds with greater precision, as well as those for 4F-indole.

It should be noted that in a Trp side chain, indole is attached to the backbone Cα by way of a methylene carbon (Cβ), which replaces the indole H3. Here the partial charges were not adjusted for this difference in structure. Instead, Cβ was relocated to the position of the indole H3 (without changing the three-dimensional position of the side chain with respect to the channel) to retain the electrostatic configuration, and the two methylene hydrogens were given zero charge.

The atom positions were taken from the optimized solid-state NMR structure for the gA dimer (PDB accession number 1mag) after rotation by 90° about the y axis and −8° about the x axis to align the channel axis with the z axis. Side-chain bond lengths and angles were reasonably close to those in the optimized ab initio geometry (RMSD < 0.04 Å for all but the F and Cβ atoms), yielding a nearly identical side-chain dipole. When side-chain torsions were varied from those in 1mag for the libration study (see below), the rigid body rotation was performed about the 1mag bonds before the Cβ relocation.

In the fluoro-Trp peptides the fluorine was positioned at the locus of the hydrogen it replaced rather than one C-F bond length from the indole C. This expedient had a small effect on the side-chain dipole moment and angle, reducing the dipole moment by up to 10% (5F-indole) and rotating the dipole as much as 4.4° (6F-indole). Furthermore, the net dipole moment varied slightly (<0.1 D) from side chain to side chain due to slight differences in side-chain internal coordinates inherent in 1mag. The ab initio indole and F-indole dipole moments, those due to the partial charges obtained by electrostatic field fitting, and the average dipole moment of the four side chains actually used (after positioning the fitted partial charges at the 1mag atom positions) is reported in the last three rows of Table 1.

Interactions with the backbone atoms for the Trp residues, the remaining amino acids, and terminators were not computed. TIP3P parameters were used for the water molecules (Jorgensen et al., 1983).

System structure

The system is illustrated diagrammatically in Fig. 1. It is based on a single gramicidin dimer using PDB coordinates for 1mag (which is centered on the origin) after the above-mentioned realignment. Through the use of image side chains (Dorigo et al., 1999), the channel is effectively embed-

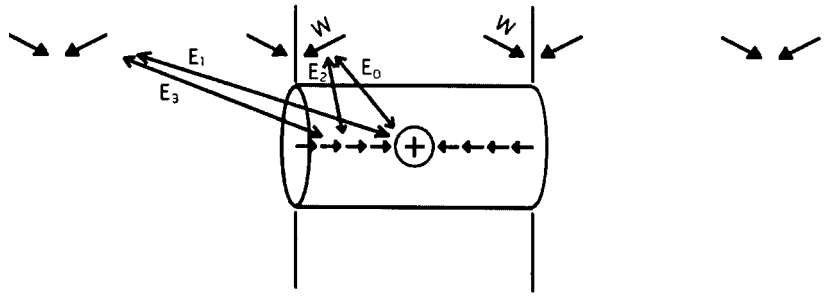

FIGURE 1 The system geometry. A single-stranded helical gramicidin A dimer (PDB structure 1mag, represented in this diagram by a cylinder) is aligned along the z axis perpendicular to a bilayer (represented by vertical lines). One of the four pairs of Trp side chains is represented by the pair of dipoles labeled W. Low-order Trp image dipole arrows are illustrated in the bulk aqueous solution. A (Na^+) ion is positioned at 2.8- or 2.9-Å intervals along the z axis. Two hemi-columns of waters each are positioned on each side of the ion, with the centers of the two neighboring oxygens at 2.8 or 2.9 Å from each other and from the center of the ion. Only four of the eight waters in the hemi-columns, those that would be included in the interaction energy with the ion at the channel center, are shown. The water columns are moved with the ion as a unit. Interaction energies defined in Eq. 1 are illustrated with long arrows.

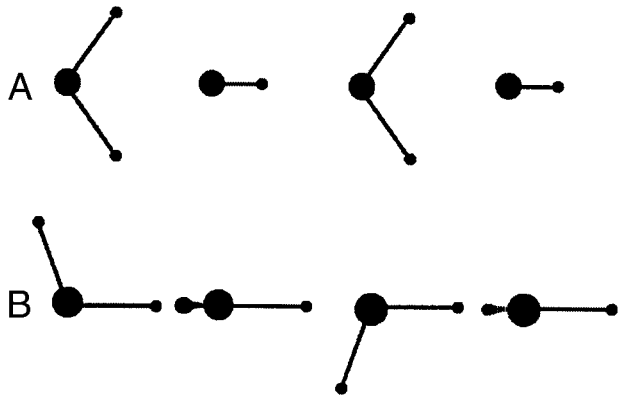

FIGURE 2 Water structure. (*a*) Herringbone pattern; (*b*) Channel hydrogen-bonded pattern. For the herringbone water pattern, oxygens are separated by 2.8 Å. Hydrogens are positioned so that the water dipoles lie on the *z* axis. Adjacent water planes are orthogonal to each other. In the channel hydrogen-bonded structure, the oxygens are separated by 2.9-Å intervals. One hydrogen is positioned on the axis and the other in such a way that consecutive water planes rotate about the axis in 90° increments.

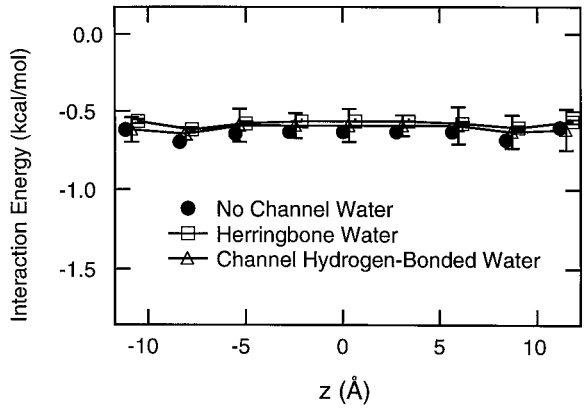

FIGURE 3 Contribution of the channel water to the potential energy of interaction between the (two) Trp_{13} side chains (with their images in bulk water) and the channel contents: ●, interaction of the side chains and images with the ion alone. The other two curves show the interaction of side chain and images with the ion and a column of waters oriented in either the channel hydrogen-bonded structures (△) or the herringbone pattern (□). Variation bars represent ±1 SD of the interaction energy among water column rotations.

ded in a 33-Å bilayer of dielectric constant $\epsilon = 2$, appropriate for monoolein/*n*-hexadecane bilayers (Dilger et al., 1982). The dielectric response of the bulk water ($\epsilon = 80$) to the polar side chains is represented with images through the fourth order. The system of image charges in a universal medium of $\epsilon = 2$ replaces the original two-dielectric system.

The channel contains one of two idealized columns, each consisting of 16 waters and an ion (eight waters on each side of the ion). These were designed following the method of Hao et al. (1997) to be readily translocated as a unit, i.e., with the ion and water oxygens located on the channel (*z*) axis. Throughout the computation, only eight of the waters and one ion are ever located in the interior of the channel, and only these are included in the interaction energies. In both idealized columns, the water dipoles retain a fixed angle with the channel axis throughout column translations and rotations. In the herringbone pattern (Fig. 2 *a*), water dipoles are aligned with the *z* axis and point toward the ion with the planes of adjacent waters orthogonal to each other. In the channel hydrogen-bonded pattern (Fig. 2 *b*) each water dipole forms an angle of 52.25° with the channel axis. In this case, adjacent water planes are rotated by 90° increments, forming a helical pattern with a rise of four water molecules per turn.

Finally, the other major components of the real system are the interfacial polar headgroups, which are assumed to be invariant and therefore are not included here.

Computational procedure

The interaction energy *E* was computed according to Eq. 1:

$$E = E_0 + E_1 + E_2 + E_3, \qquad (1)$$

where E_0 is the ion/side-chain interaction energy, E_1 is the ion/image interaction energy, E_2 is the channel water side-chain interaction energy, and E_3 is the channel water/image interaction energy. The ion and water columns were moved together in discrete intervals of 2.9 Å for the herringbone water pattern and 2.8 Å for the channel hydrogen-bonded water pattern. The ion started at the origin and was moved in both *z* directions until reaching ±11.6 Å for the herringbone pattern, ±11.2 Å for the channel hydrogen-bonded pattern. At each of the nine discrete positions, the entire idealized column was rotated 360° about the *z* axis in 30° increments. This allowed an estimate of how variations in column structure might affect interaction energy. The mean and standard deviation of *E* were computed for the energies at each discrete position, the standard deviation being plotted as variation bars.

Effects of side-chain librations on *E* were estimated by changing χ_2 for Trp_9, Trp_{11}, Trp_{13}, or Trp_{15} by ±25°, ±29°, ±26°, or ±19°, respectively (Hu et al., 1995). Effects of the lipid environment and fluorination on average side-chain positions were shown by solid-state NMR to be small but measurable (Cotten et al., 1999). To sample these effects, we computed *E* for one case, 5F-Trp_{13} in dioleoylphosphatidylcholine (DOPC), using the side-chain dihedral angles measured by Cotten et al. (1999): $\chi_1 = 299°$ and $\chi_2 = 261°$. These contrast with the 1mag dihedrals for Trp_{13}: $\chi_1 = 296°$ and $\chi_2 = 273°$.

All computations were performed with the molecular modeling program CHARMM v. 24 (Brooks et al., 1983), with structure building, manipulation, and visualization performed using QUANTA (Molecular Simulations, San Diego, CA).

RESULTS

The ion Trp and ion image interaction energies ($E_0 + E_1$) for 5F-Trp_{13} gA, obtained using the ab initio charges in the 1mag positions, were ~−0.6 kcal/mol throughout the channel as shown in Fig. 3 (filled circles). Addition of the interactions with the channel waters yields the total energy (*E*), shown for each of the two types of idealized water columns as open symbols. The reduction in interaction energy magnitude is greater for the herringbone pattern (open squares) where it reaches 11% than for the channel hydrogen-bonded arrangement (open triangles) where the maximum reduction is 8%, but in both cases, the reduction in magnitude is fairly constant throughout the channel. Similar reductions were seen for all the other cases computed, so we hereafter report only *E*, the total interaction energy. Also, because the majority of waters in a channel are expected to be in the channel hydrogen-bonded pattern and the effects of the two columns are similar, subsequent

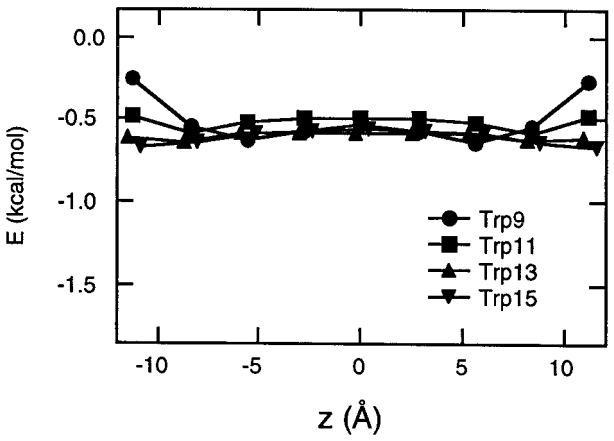

FIGURE 4 Total interaction energy (ion and channel hydrogen-bonded water column with side-chain pair and images) for each Trp pair in the 1mag configuration. ●, Trp_9; ■, Trp_{11}; ▲, Trp_{13}; ▼, Trp_{15}.

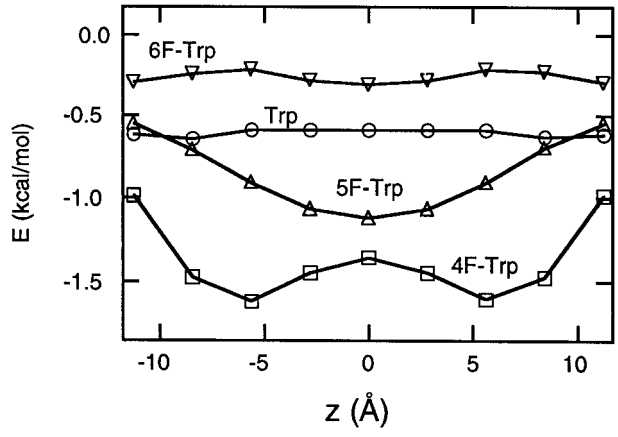

FIGURE 5 Effects of ring fluorination position on total interaction energy (ion and channel hydrogen-bonded water column with Trp_{13} side chain pair and images) for 4F- (□), 5F- (△), 6F- (▽), and native Trp_{13} (○). In each case, the side chains are positioned in the 1mag conformation.

plots show only the value of E computed using the channel hydrogen-bonded column energies.

It should be noted that for both water structures, but especially for the four-fold symmetric channel-hydrogen-bonded water column, the channel-water/side-chain interaction energy varied somewhat with axial rotations of the idealized column. The variation bars are intended to provide some idea of the uncertainty in the channel-water/Trp and Trp image interaction energy resulting from variations in water structure. The variations were examined for all cases, but those shown in Fig. 3 were found to be representative, so variation bars are omitted in the energies plotted in all subsequent figures.

In Fig. 4 the total interaction energy is shown for each of the four native Trp pairs. Trp_{11} produces slightly less stabilization at the center of the channel, but otherwise the interactions are similar at the center. The main differences appear at and external to the binding site, where Trp_9 and Trp_{11} yield significantly less stabilization than Trp_{13} and Trp_{15}.

Fluorination can either enhance or reduce stabilization depending on the position of the fluorine on the indole, as illustrated using the Trp_{13} pair potential in Fig. 5. For this purpose, the side-chain structure was not altered from the 1mag positions, although slight changes in side-chain position have been measured for 5F and 6F analogs (Cotten et al., 1999). In comparison with the Trp_{13} trace (shown in Fig. 4 and redrawn as open circles in Fig. 5), 5-fluorination strengthens the interaction energy at the channel center by 0.53 kcal/mol and 4-fluorination by 0.77 kcal/mol, whereas 6-fluorination weakens the interaction by 0.27 kcal/mol. There are also interesting differences between the analogs at the binding site (9.5–12.5 Å from the bilayer center), where 5-fluorination has only a minor effect on interaction energy, whereas 6-fluorination still reduces interaction energy and 4-fluorination dramatically enhances interaction energy.

The dependence of the fluorination effect on the amino acid number (again without taking into effect changes in side chain orientation induced by fluorination) is illustrated in Fig. 6 where the total potentials for interactions with Trp pairs 9, 11, 13, and 15 are plotted together. 5F-Trp potentials are shown in Fig. 6 *a*, 6F-Trp in Fig. 6 *b*, and 4F-Trp in Fig. 6 *c*. For 5-fluorination, the interaction energy profiles are parabolic with increasing effects for the more external Trps. For 6-fluorination, the profiles are flat, again with increasing effects for the more external Trps. The net free energy changes induced by fluorination (assuming no change in side-chain structure or dynamics) at key sites in the transport pathway are given for 5-fluorination in Table 2 and for 6-fluorination in Table 3. For all four peptides, 5-fluorination should principally reduce the central barrier whereas 6-fluorination should mainly decrease the ion-binding affinity of the channel, i.e., reduce the exit barrier. The pattern for 4-fluorination is much more variable with the profile evolving from a double well shape, deepest at the binding site and highest in the center for Trp_{15}, to a parabolic well with the least impact at the binding site and greatest depth at the center for Trp_9. This translates into a complex pattern of changes at the key sites (Table 4).

Fluorination-induced changes in average side-chain position are expected to modify the interaction potentials. To estimate the magnitude of this effect, we have computed the potentials for 5F-Trp_{13} positioned as measured for this analog in DOPC bilayers (Cotten et al., 1999). This represented the worst-case deviation from the 1mag positions of those measured, which also included 5F and 6F analogs of Trps 11, 13, and 15 in DMPC bilayers. Fig. 7 demonstrates that the small average change in side-chain position upon 5-fluorination and bilayer thickening should cause only a modest deepening of the interaction energy profile.

On the other hand, torsional librations are measured to be up to $\pm 29°$, primarily about χ_2. These have quite a large

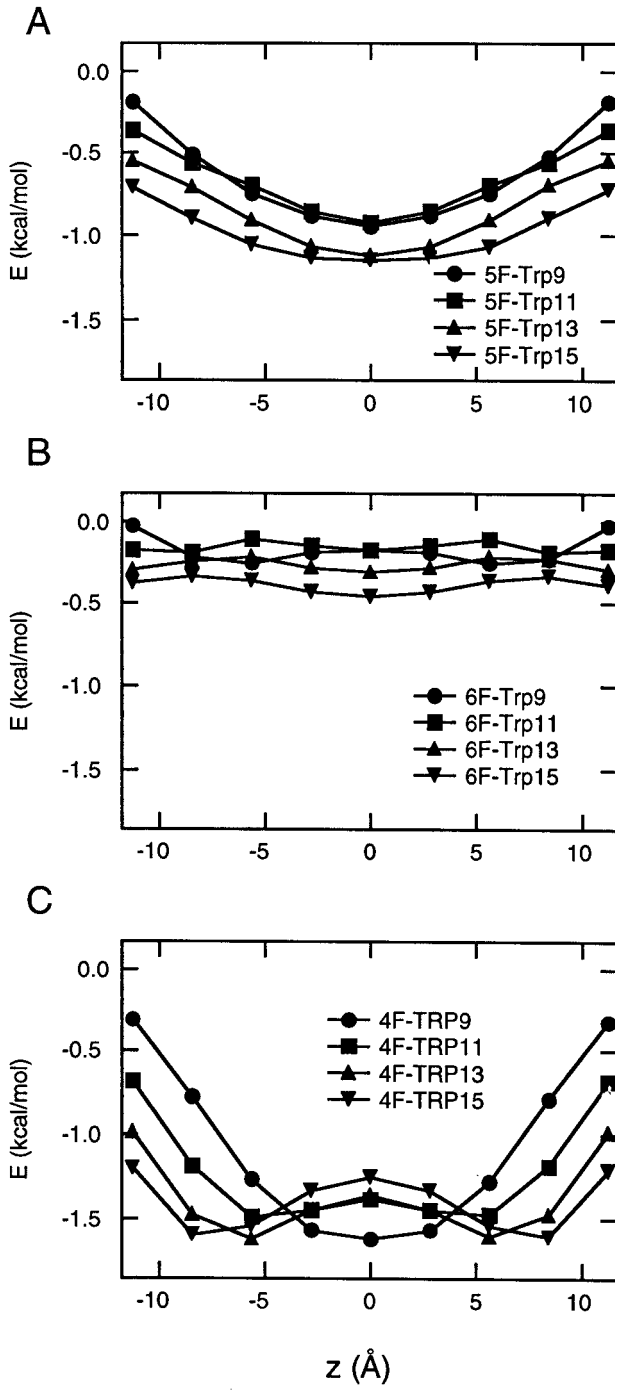

FIGURE 6 Comparison of fluorination effects on total interaction energy (ion and channel hydrogen-bonded water column with side-chain pairs and images) at the four different residues. (*a*) 5F mutations of pairs of Trp_9 (●), Trp_{11} (■), Trp_{13} (▲), and Trp_{15} (▼); (*b*) 6F mutations of the four individual Trp pairs (same symbols as *a*); (*c*) 4F mutations of the four individual Trp pairs (same symbols as *a*).

impact on the interaction energy profile. The libration effects are further amplified in the fluorinated peptides where the dipole moment is greater than that of the native Trp. Fig. 8 summarizes the change in interaction energy as a consequence of positive or negative libration (about the 1mag positions) for each case studied. The figure contains one panel for each amino acid species, Trp or one of its three fluorinated analogs. Each panel shows five sets of changes representing the five ion positions in the channel. Each set has eight bars, four light bars for the negative rotations about χ_2 and four dark bars for the positive rotations about χ_2. The four pairs of bars represent, from left to right, changes due to librations at positions 9, 11, 13, or 15 respectively. In each case, we have used libration amplitudes for gA from solid-state NMR (Hu and Cross, 1995), namely 25°, 26°, 29°, and 19° for Trps 9, 11, 13, and 15, respectively.

Three trends in the libration effects can be discerned: 1) effects are greater near the binding site (9.5–12.5 Å) than at the center of the channel; 2) negative librations frequently increase the favorable interactions and positive librations reduce them; and 3) librations of residues near the center of the channel have greater effects than those near the mouth. Thus, binding energy is more affected by side-chain dynamics than the translocation barrier, and movements of Trp_9 should cause larger distortions in the energy profile than those of Trp_{15}.

TABLE 2 Free energy changes for 5-fluorination

	6F-Trp_9	6F-Trp_{11}	6F-Trp_{13}	6F-Trp_{15}
$\Delta E_{binding}$	0.23	0.31	0.31	0.28
ΔE_{center}	0.36	0.32	0.27	0.11
$\Delta E_{center} - \Delta E_{binding}$	0.13	−0.01	−0.05	−0.17

ΔE is the difference in potential energy (kcal/mol) between the bilateral pair of fluorinated analogs and Trp. The first row contains the difference at 11.2 Å, near the location of the binding site (9.5–12.5 Å). The second row contains the difference at 0 Å, the center of the channel. The third row is the difference between the first and second rows and represents the change in the translocation barrier, assuming it peaks at the center.

DISCUSSION

The native Trp potentials in Fig. 4 are similar to previous results (Fig. 6, o1 positions in Dorigo et al. (1999)), despite the usage of ab initio charges that more accurately represent the indole dipole moment. This is surprising because the toph19 partial charges used there yielded a net side-chain dipole moment of only 1.15 D compared with the net moment of the charges used here, 2.0 D. On the basis of the

TABLE 3 Free energy changes for 6-fluorination

	5F-Trp_9	5F-Trp_{11}	5F-Trp_{13}	5F-Trp_{15}
$\Delta E_{binding}$	0.07	0.12	0.07	−0.05
ΔE_{center}	−0.41	−0.42	−0.53	−0.57
$\Delta E_{center} - \Delta E_{binding}$	−0.48	−0.54	−0.60	−0.52

*Symbols have same meaning as in Table 2.

TABLE 4 Free energy changes for 4-fluorination

	4F-Trp$_9$	4F-Trp$_{11}$	4F-Trp$_{13}$	4F-Trp$_{15}$
$\Delta E_{binding}$	−0.06	−0.20	−0.38	−0.54
ΔE_{center}	−1.08	−0.88	−0.77	−0.68
$\Delta E_{center} - \Delta E_{binding}$	−1.02	−0.68	−0.39	−0.14

Symbols have same meaning as in Table 2.

low dipole moment, Dorigo et al. (1999) concluded that the interaction between ion and side chain (including side-chain images) should reach a nadir of −0.9 kcal/mol in the center of the channel for each of the four Trp pairs.

In fact, the Trp potentials are slightly more negative due to the strengthened dipole moments, but not as much as expected. Because Dorigo et al. (1999) used the solution-state NMR structure rather than the solid-state NMR structure used here, we checked whether the toph19 partial charges would produce a significantly different interaction energy profile in the 1mag structure. The profile of the ion/side-chain interaction energy (including side-chain images) with the toph19 charges in the 1mag positions was essentially the same as that reported in Dorigo et al. (1999) for the solution-state NMR structure and as that obtained here with ab initio partial charges (data not shown). We therefore conclude that the increased dipole moment obtained using ab initio partial charges did not proportionately increase the interaction energy, presumably due to higher-order multipole effects. (A similar conclusion was reached when parm22 charges from the CHARMM force field were used, as is discussed below.) In addition, the slight increase due to the increased indole dipole is offset by the newly included column-water effects. In summary, we estimate that the ion/side-chain interaction energy at the center of the channel, taking into account the bulk and channel water

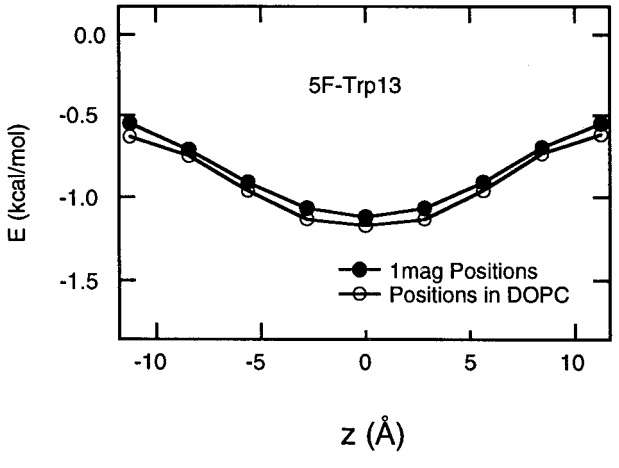

FIGURE 7 Effects of rotations caused by 5-fluorination of Trp$_{13}$ in DOPC observed in ref. 13. ●, interaction energies computed using 5F-Trp$_{13}$ in 1mag positions; ○, interaction energies computed using 5F-Trp$_{13}$ after rotations of χ_1 and χ_2 to those determined in DOPC bilayers using solid-state NMR [13].

effects, should be between −0.5 and −0.6 kcal/mol for each of the four Trp pairs (Fig. 4). For instance, the total interaction energy reaches a nadir in the center of the channel at −0.58 kcal/mol for the Trp$_{13}$ dimer pair.

For these computations, because the ion is likely to deviate an uncertain amount from the axis outside the channel and to be heavily shielded by the bath, the interaction energies were computed only for ion positions inside the channel. We expect the interaction energy to approach zero for ion positions outside of the channel, although there could be a small overshoot due to the positive end of the dipole. However, any such positive potential should largely be shielded (Sancho and Martínez, 1991).

The profile in Fig. 3 can thus be used to consider the stabilizing effects of the Trp$_{13}$ side chains at key positions in the channel, such as at the binding site and at the center. The underlying free energy profile for ion transport is thought to be a square well modified by a rise at the channel center due to image and interface dipole potentials (Jakobsson and Chiu, 1987). Therefore, the ion's negative interaction energy with Trp$_{13}$ at the binding site would increase the binding affinity through a reduction in the exit rate constant. From Fig. 3, the Trp$_{13}$ dipole should increase the exit barrier by ~0.6 kcal/mol. However, the interaction energy changes but little between the binding site and the center of the channel, so that, under the usual assumption that the peak height of the translocation barrier occurs at the center of the channel, Trp$_{13}$ is predicted to have no effect on the translocation rate.

Woolf and Roux (1997) report dynamic average Trp-side-chain/ion interaction energies for gA that were more localized to the binding site (and with little effects at the transition barrier) than the average structure potential energies reported here and in Dorigo et al. (1999). It is possible that this discrepancy is partly due to nonlinear averaging of the librating structure energies. However, to more carefully evaluate the origin of this difference, we directly compared the axial ion-side chain interaction energy profiles from CHARMM all22 force field utilized by Woolf and Roux (1997) to the one obtained with ab initio partial charges but the same peptide structure used here (that of 1mag, with the channel axis reoriented along the z axis). It was found that the all22 charges yielded interaction energy profiles similar to the published Woolf and Roux ensemble average profile (results not shown). The all22 side-chain dipole potential has about the same magnitude and angle as does the ab initio charge set used here. Thus, again the profile shape is determined not just by the dipole moment, but by higher multipole moments as well.

Our ab initio charges were obtained for indole in a vacuum. The Trp side chain may be significantly polarized in the polar headgroup environment, changing the multipole moments. Furthermore, we noticed that ion movements off axis could have considerable effects on the profile features, which could be especially important for small ions like

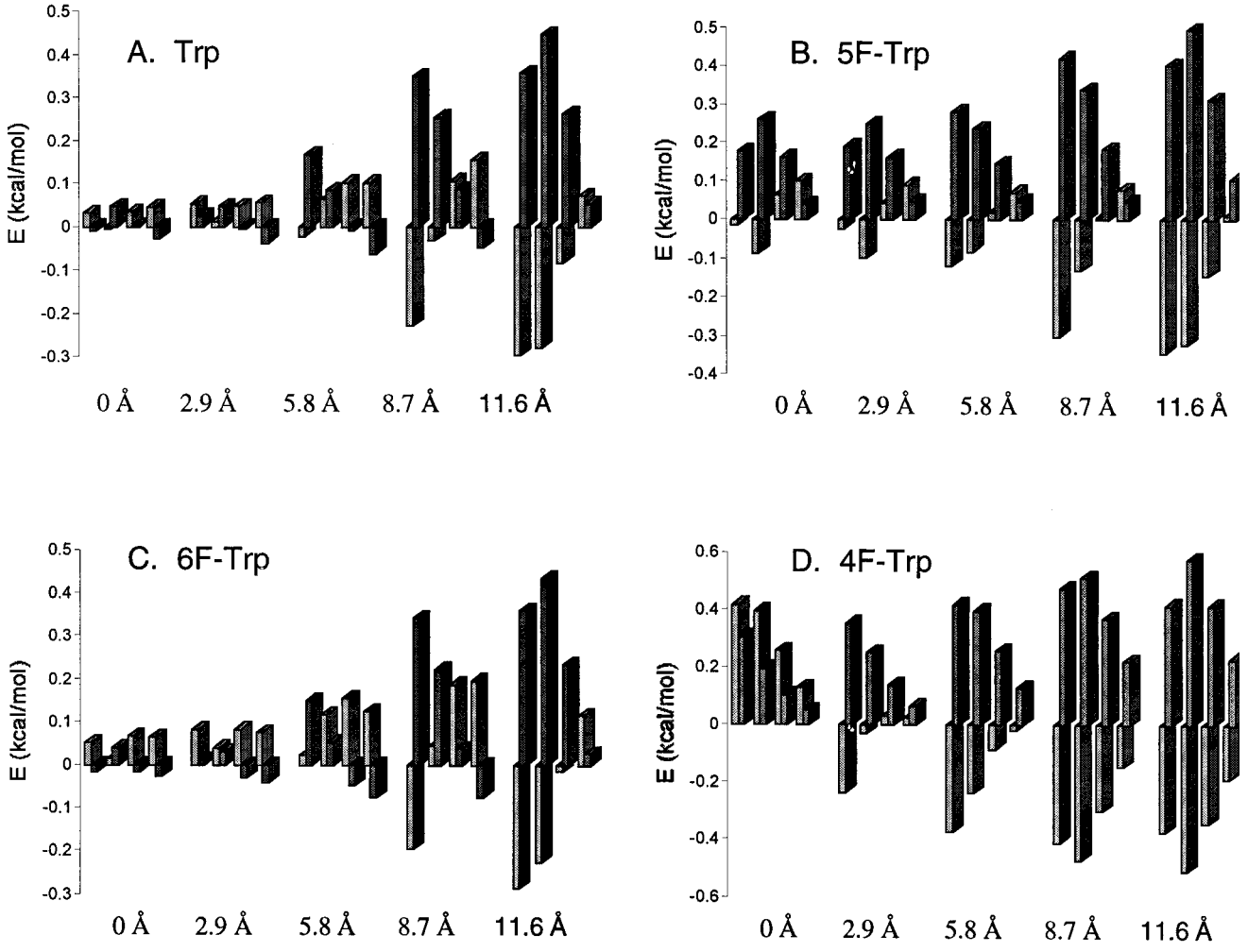

FIGURE 8 Bar plots of the ΔE for librations (positive and negative in χ_2) for Trp_{13} (*a*), 5F-Trp_{13} (*b*), 6F-Trp_{13} (*c*), and 4F-Trp_{13} (*d*) For each panel, the effects of negative (lighter bar on the left) and positive (darker bar on the right) librations at positions 9, 11, 13, and 15 are compared at the five intra-channel sites 0, +2.9, +5.8, +8.7, and +11.6 Å. (The values at the mirror image ion positions, −2.9, −5.8, −8.7, and −11.6 Å, were nearly identical to those shown).

Na^+, Li^+, and H^+. Also, our observation that Trp should enhance ion binding rather than reduce the net translocation barrier predicts that, compared with Phe, for instance, Trp should reduce conductance rather than increase it, contrary to observation (Becker et al., 1991) and theory (Hu and Cross, 1995). It is therefore important to use the current results with caution. However, initial data analysis suggests that the potential profile obtained with the ab initio charges for 5F-indole are correct in identifying the main locus of 5F-Trp effects at the center of the channel (Thompson et al., 2001).

Fluorination of the Trp indole C5 carbon increases the side-chain dipole moment by a factor of 1.9 compared with native Trp and considerably enhances the interactions with the ion, especially at the center of the channel. Fluorination of the indole C4 should cause a yet greater effect at the center of the channel, whereas fluorination at position C6 reduces the interaction throughout the permeation pathway ~2-fold. Slight changes in the average side-chain position occasioned by fluorination or change in lipid bilayer thickness only have small effects on the potential energy profile. However, the large thermal librations shown to occur about the side-chain torsions (Hu et al., 1995) should cause large dynamic changes in the interaction energy profile, especially near the binding sites. The librations may not be symmetrical about the average position but would be populated according to the energy. Our main purpose here is only to illustrate the potential energy components of these various possible effects. However, it might be interesting to consider the role of these librations further from both the point of view of their effect on the energy profile and also how ion occupancy might bias side-chain position. For instance, from our results one might speculate that ions in

the binding sites might induce negative side chain rotations, especially for Trp_9 and Trp_{11}, which in turn would further stabilize ion binding.

The effects of 5- and 6-fluorination on channel conductance have now been carefully measured for each individual gA Trp (Busath et al., 1998; Cotten et al., 1999; C. D. Cole, A. S. Frost, N. Thompson, M. Cotten, T. A. Cross, and D. D. Busath, submitted). The side-chain structure has been determined in DMPC multilayers for 5- and 6-fluorinated Trps 11, 13, and 15 gA, and in DOPC multilayers for 5F-Trp_{13} gA, and only modest changes in average position were noted (Cotten et al., 1999). The single-channel currents for 5F-Trp_{13} gA were found to be increased compared with native gA in DPhPC bilayers, but they were reduced in GMO bilayers except at the highest ion concentration used (2 M) (Busath et al., 1998). Kinetic modeling (Thompson et al., 2001) indicates that this result is consistent with the assumption that energetic changes of the magnitude computed here are occurring in both cases but that in GMO bilayers the transport is limited more by exit in the 0.1–1.0 M salt range whereas in lecithin bilayers translocation is more limiting. This has been ascribed to the increased interfacial dipole potential of lecithin bilayers (Busath et al., 1998; Thompson et al., 2001).

To compare these experimental results with the computations presented here, the difference between the total interaction energy with the fluorinated side chain and that with the Trp side chain at key points in the permeation pathway, namely, the binding site and the center of the channel, were given in Tables 2–4. We approximate the location of the diffuse binding site as 11.2 Å, a point on our grid reasonably well centered in the range determined by Tian and Cross (1999), 9.5–12.5 Å. The tables each give the energy difference at the binding site (which represents the change in exit barrier assuming no entry barrier or no change in entry barrier), the center of the channel, and the difference between that at the center and the binding site (which represents the change in translocation barrier). Fig. 6 *b* shows that 6-fluorination of one pair of the Trp side chains should decrease interaction energy throughout the course of permeation. This has the effect of reducing the Trp-induced increase in the exit barrier by a factor of ~2. This is shown in the first row of Table 2. The translocation barrier change (the potential energy difference at the center of the channel relative to that at the binding site) is negligible (Table 2, row 3).

In contrast to the 6-fluorination effects, 5-fluorination reduces the translocation barrier (Table 3, row 3) with negligible effects on the binding energy, and thus on the exit barrier (Table 3, row 1), consistent with the kinetic modeling of the 5F-Trp_{13} data (Thompson et al., 2001). Thus, the 5F- and 6F-compounds are predicted to have distinct effects, the one primarily reducing the translocation barrier, the other primarily increasing the exit barrier.

A much more complex pattern is expected for 4F-Trp compounds (Table 4). Unlike the 5F- and 6F-compounds, these results predict that the 4-fluorination effects would depend very heavily on the amino acid position in the peptide sequence. The translocation barrier is increasingly reduced as fluorination is applied to residues located deeper in the bilayer (Table 4, row 3, reading from right to left), whereas the exit barrier is decreasingly reduced (Table 4, row 1). It should be very interesting to examine the conductance properties of 4F-compounds because, according to the electrostatic computations presented here, both the shape and size of the translocation energy barrier should be greatly affected by the side chains in ways that depend heavily on the side-chain position.

SUMMARY

The ion/side-chain interaction energies were computed for native and fluorinated gA analogs at each of the four sequence positions. Interaction energies at the center of the channel were ~ -0.6 kcal/mol for each of the four native Trp pairs, increased nearly 2-fold and 3-fold, respectively, for 5- and 4-fluorination and reduced nearly 2-fold for 6-fluorination. The effects depend somewhat on the Trp sequence position, especially for the 4F analogs. Librations modulate the interaction energy at the binding site, especially for Trp_9 and Trp_{11} where they can modify interaction energy by $\sim \pm 0.4$ kcal/mol, but they have little effect at the center of the channel. 5-Fluorination should increase the translocation rate with minor effects on the exit rate, whereas 6-fluorination should enhance the exit rate with almost no effects on translocation.

We thank Stephen Markham, Jeff Markham, and Adam Frost for assistance with figure preparation and Prof. Mark F. Schumaker for helpful suggestions. We are especially grateful to Benoit Roux who provided us with his analysis of the ion side-chain interaction energy profile for our comparison and to Vivek Ramakrishnan for assisting with this comparison.

This project was supported by National Institutes of Health R01 AI23007 to T.A.C. and D.D.B.

REFERENCES

Andersen, O. S. 1983. Ion movement through gramicidin A channels: single-channel measurements at very high potentials. *Biophys. J.* 41: 119–133.

Andersen, O. S., D. V. Greathouse, L. L. Providence, M. D. Becker, and R. E. Koeppe II. 1998. Importance of tryptophan dipoles for protein function: 5-fluorination of tryptophans in gramicidin A channels. *J. Am. Chem. Soc.* 120:5142–5146.

Arsenyev, A. S., A. L. Lomize, I. L. Barsukov, and V. F. Bystrov. 1990. Gramicidin A transmembrane channel: three-dimensional structural rearrangement based on NMR spectroscopy and energy refinement. *Biol. Membr.* 3:1723–1778.

Becker, D. V. Greathouse, R. E. Koeppe II, and O. S. Andersen. 1991. Amino acid sequence modulation of gramicidin channel function: effects of tryptophan-to-phenylalanine substitutions on the single-channel conductance and duration. *Biochemistry.* 30:8830–8839.

Brooks, B. R., R. E. Bruccoleri, B. D. Olafson, D. J. States, S. Swaminathan, and M. Karplus. 1983. CHARMM: a program for macromolec-

ular energy, minimization, and dynamics calculations. *J. Comput. Chem.* 4:187–217.

Busath, D. D. 1993. The use of physical methods in determining gramicidin channel structure and function. *Annu. Rev. Physiol.* 55:473–501.

Busath, D. D., C. D. Thulin, R. W. Hendershot, L. R. Phillips, P. Maughn, C. D. Cole, N. C. Bingham, S. Morrison, L. C. Baird, R. J. Hendershot, M. Cotten, and T. A. Cross. 1998. Non-contact dipole effects on channel permeation. I. Experiments with (5F-indole)Trp-13 gramicidin A channels. *Biophys. J.* 75:2830–2844.

Cifu, A. S., R. E. Koeppe II,, and O. S. Andersen. 1992. On the supramolecular organization of gramicidin channels: the elementary conducting unit is a dimer. *Biophys. J.* 61:189–203.

Cotten, M., C. Tian, D. D. Busath, R. B. Shirts, and T. A. Cross. 1999. Modulating dipoles for structure-function correlations in the gramicidin A channel. *Biochemistry.* 38:9185–9197.

De Wall, S. L., E. S. Meadows, L. J. Barbour, and G. W. Gokel. 2000. Synthetic receptors as models for alkali metal cation-pi binding sites in proteins. *Proc. Natl. Acad. Sci. U.S.A.* 97:6271–6276.

Dilger, J. P., L. R. Fisher, and D. A. Haydon. 1982. A critical comparison of electrical and optical methods for bilayer thickness determination. *Chem. Phys. Lipids.* 30:159–176.

Dorigo, A. E., D. G. Anderson, and D. D. Busath. 1999. Noncontact dipole effects on channel permeation. II. Trp conformations and dipole potentials in gramicidin A. *Biophys. J.* 76:1897–1908.

Duca, K. A., and P. C. Jordan. 1998. Comparison of selectively polarizable force fields for ion-water-peptide interactions: ion translocation in a gramicidin-like channel. *J. Phys. Chem. B* 102:9127–9138.

Fairbanks, T. G., C. L. Andrus, and D. D. Busath. 1999. Lorentzian noise in single gramicidin A channel formamidinium currents. *In* Proceedings of the Novartis Foundation Symposium 225: Gramicidin and Related Ion Channel-Forming Peptides. John Wiley and Sons, Chichester, UK. 74–87.

Fonseca, V., P. Daumas, L. Ranjalahy-Rasoloarijao, F. Heitz, R. Lazaro, Y. Trudelle, and O. S. Andersen. 1992. Gramicidin channels that have no tryptophan residues. *Biochemistry.* 31:5340–5350.

Hao, Y., M. R. Pear, and D. D. Busath. 1997. Molecular dynamics study of free energy profiles for organic cations in gramicidin A channels. *Biophys. J.* 73:1699–1716.

Heitz, F., P. Daumas, N. Van Mau, R. Lazaro, Y. Trudelle, C. Etchebest, and A. Pullman. 1988. Linear gramicidins: influence of the nature of the aromatic side chains on the channel conductance. *In* Transport Through Membranes: Carriers, Channels, and Pumps. Kluwer Academic Publishers, Boston. 147–165.

Heitz, F., C. Gavach, G. Spach, and Y. Trudelle. 1986. Analysis of the ion transfer through the channel of 9,11,13,15-phenylalanylgramicidin A. *Biophys. Chem.* 24:143–148.

Hladky, S. B. 1999. Can we use rate constants and state models to describe ion transport through gramicidin channels? *In* Proceedings of the Novartis Foundation Symposium 225: Gramicidin and Related Ion Channel-Forming Peptides. John Wiley and Sons, Chichester, UK. 93–107.

Hladky, S. B., and D. A. Haydon. 1984. Ion movements in gramicidin channels. *Curr. Top. Membr. Transport.* 21:327–372.

Hu, W., and T. A. Cross. 1995. Tryptophan hydrogen bonding and electrical dipole moments: functional roles in the gramicidin channel and implications for membrane proteins. *Biochemistry.* 34:14147–14155.

Hu, W., N. D. Lazo, and T. A. Cross. 1995. Tryptophan dynamics and structural refinement in a lipid bilayer environment: solid state NMR of the gramicidin channel. *Biochemistry.* 34:14138–14146.

Hu, W., K. C. Lee, and T. A. Cross. 1993. Tryptophans in membrane proteins: indole ring orientations in the gramicidin channel. *Biochemistry.* 32:7035–7047.

Jakobsson, E., and S.-W. Chiu. 1987. Stochastic theory of ion movement in channels with single-ion occupancy. *Biophys. J.* 52:33–45.

Jorgensen, W. L., J. Chandrasekhar, J. D. Madura, W. Imprey, and M. L. Klein. 1983. Comparison of simple potential functions for simulating liquid water. *J. Chem. Phys.* 79:926–935.

Ketchem, R. R., B. Roux, and T. A. Cross. 1997. High-resolution polypeptide structure in a lamellar phase lipid environment from solid state NMR derived orientational constraints. *Structure.* 5:1655–1669.

Killian, J. A. 1992. Gramicidin and gramicidin-lipid interactions. *Biochim. Biophys. Acta.* 1113:391–425.

Kim, K. S., D. P. Vercauteren, M. Welti, S. Chin, and E. Clementi. 1985. Interaction of K^+ ion with the solvated gramicidin A transmembrane channel. *Biophys. J.* 47:327–335.

Koeppe, R. E., J. A. Killian, and D. V. Greathouse. 1994. Orientations of the tryptophan 9 and 11 side chains of the gramicidin channel based on deuterium nuclear magnetic resonance spectroscopy. *Biophys. J.* 66: 14–24.

Koeppe, R. E., J. A. Killian, T. C. B. Vogt, B. de Kruijff, M. J. Taylor, G. L. Mattice, and D. V. Greathouse. 1995. Palmitoylation-induced conformational changes of specific side chains in the gramicidin transmembrane channel. *Biochemistry.* 34:9299–9306.

Koeppe, R. E., J. L. Mazet, and O. S. Andersen. 1990. Distinction between dipolar and inductive effects in modulating the conductance of gramicidin channels. *Biochemistry.* 29:512–520.

Koeppe, R. E., T. C. B. Vogt, D. V. Greathouse, J. A. Killian, and B. de Kruijff. 1996. Conformation of the acylation site of palmitoylgramicidin in lipid bilayers of dimyristoylphosphatidylcholine. *Biochemistry.* 35: 3641–3648.

Olah, G. A., H. W. Huang, W. Liu, and Y. Wu. 1991. Location of ion-binding sites in the gramicidin channel by x-ray diffraction. *J. Mol. Biol.* 218:847–858.

Phillips, L. R., C. D. Cole, R. J. Hendershot, M. Cotten, T. A. Cross, and D. D. Busath. 1999. Noncontact dipole effects on channel permeation. III. Anomalous proton conductance effects in gramicidin. *Biophys. J.* 77:2492–2501.

Roux, B., B. Prod'hom, and M. Karplus.1995. Ion transport in the gramicidin channel: molecular dynamics study of single and double occupancy. *Biophys. J.* 68:876–892.

Russell, E. W. B., L. B. Weiss, F. I. Navetta, R. E. Koeppe II, and O. S. Andersen. 1986. Single-channel studies on linear gramicidin with altered amino acid side chains: effects of altering the polarity of the side chain at position 1 in gramicidin A. *Biophys. J.* 49:673–686.

Sancho, M., and G. Martínez. 1991. Electrostatic modeling of dipole-ion interactions in gramicidin like channels. *Biophys. J.* 60:81–88.

Thompson, N. G., C. D. Cole, M. Cotten, T. A. Cross, and D. D. Busath. 2001. Noncontact dipole effects on channel permeation. IV. Kinetic model of 5F-Trp_{13} gramicidin A currents. *Biophys. J* 81:1245–1254.

Tian, F., and T. A. Cross. 1999. Cation transport: an example of structural based selectivity. *J. Mol. Biol.* 285:1993–2003.

Tian, F., K.-C. Lee, W. Hu, and T. A. Cross. 1996. Monovalent cation transport: lack of structural deformation upon cation binding. *Biochemistry.* 35:11959–11966.

Urry, D. W., K. U. Prasad, and T. L. Trapane. 1982. Location of monovalent cation binding sites in the gramicidin channel. *Proc. Natl. Acad. Sci. U.S.A.* 79:390–394.

Woolf, T. B., and B. Roux. 1997. The binding site of sodium in the gramicidin A channel: comparison of molecular dynamics with solid-state NMR data. *Biophys. J.* 72:1930–1945.

Woolley, G. A., and B. A. Wallace. 1992. Model ion channels: gramicidin and alamethicin. *J. Membr. Biol.* 129:109–136.